PART II: REFERENCE

1 COMPONENT SUMMARY

This section contains brief descriptions of the major components in Streamer. Other sections in this reference guide provide additional details.

Two radiative transfer solvers are used in *Streamer*: a two-stream method and a discrete ordinate solver. The discrete ordinate solver, called DISORT, is described in Stamnes et al. (1988) and has been available to the public as a stand-alone package for many years. Starting with *Streamer* version 3, DISORT version 2 is used (Stamnes et al., 2000). The two-stream method is decribed in Toon et al. (1989). The discrete ordinate solver is the more accurate of two, and can be used to compute either radiances or fluxes. The two-stream solver computes only fluxes but is much faster than DISORT. A discussion of the two-stream accuracy is given in the *Flux and Radiance Quantities* section of this guide.

The 24 shortwave bands are the same as those in Slingo and Schrecker (1982). The parameterization of Rayleigh scattering optical depth is also from Slingo and Schrecker.

Cloud optical properties are based on parameterization schemes from three different sources. For water clouds, the data are taken from Hu and Stamnes (1993). Effective radii, the ratio of the third to the second moments of the particle size distribution, range from 2.5 to 60 microns and are given for 293 wavelengths throughout the shortwave and longwave portions of the spectrum. For ice clouds in the shortwave, the six-band parameterization of Fu and Liou (1993), based on randomly oriented hexagonal crystals, is used. Longwave ice cloud optical properties are based on Mie calculations using spherical particles for 132 wavelengths. This parameterization is unpublished but follows the methodology of Hu and Stamnes. Both the water and ice cloud parameterizations of optical properties are based on the empirical relationship between the particle effective radius and extinction, single scatter albedo, the asymmetry parameter, and the cloud water content. For radiative transfer calculations, water cloud and longwave ice cloud optical properties are averaged over *Streamer* bands.

Aerosol amounts (via extinction coefficients) can be distributed vertically either by a user-supplied profile or one of the internal standard profiles. Four profiles are available that are combinations of two tropospheric and two stratospheric loadings. The profile shapes are based on data in the LOWTRAN-7 radiative transfer model (Kneizys et al., 1988). Aerosol optical properties are based on Shettle and Fenn (1979) except for Arctic haze (Blanchet and List, 1983).

Standard profiles include tropical, mid-latitude, subarctic, and arctic. They are based on data in Ellingson et al. (1991) except for the Arctic profiles of temperature and humidity, which are based on Arctic Ocean coastal and drifting station data.

Gas data were provided by S.-C. Tsay (pers. comm., 1991; *cf.*, Tsay et al., 1989). Absorption amounts are determined with the exponential sum fitting (ESFT) technique. Only four gases are present in *Streamer*: water vapor, carbon dioxide, ozone, and oxygen.

Several spectral albedo data sets are available in *Streamer.* Sand and vegetation data are from Tanre et al. (1986); meltpond and bareice albedos are from Grenfell and Maykut (1977); open sea water data are based on Brieglieb et al. (1985); freshwater albedos are from Fresnel calculations; and snow data were computed using a four-stream model.

2 FLUX AND RADIANCE QUANTITIES

FLUXES

The broadband surface albedo is an all-sky value, calculated in the traditional manner as the ratio of the up to downwelling shortwave fluxes; i.e.,

$$\alpha_s = \frac{F_{shortwave-up}}{F_{shortwave-down}}$$

The cloud radiative effect, more commonly called "cloud forcing", is computed from the net shortwave and longwave fluxes at the surface and TOA. It is defined as

$$CF_{\lambda, z} = \int_0^{A_c} \frac{\partial F_{\lambda, z}}{\partial a} da = F_{\lambda, z}(A_c) - F_{\lambda, z}(0)$$

where $F_{\lambda,z}$ is the net flux (W m^{-2}) for shortwave or longwave radiation (Λ) at either the surface or TOA (z), and A_c is the cloud fraction in the scene. The net flux is equal to the downwelling minus the upwelling fluxes. The first term on the right side of the equation is the net flux for all-sky conditions, including clear sky. Analogous to net radiation, the all-wave net cloud forcing at either the surface or TOA is

$$CF_z = CF_{shortwave} + CF_{longwave}$$

Heating/cooling rates are computed for each layer, and are based on finite difference estimates of the flux divergence at each pair of levels:

$$\frac{\Delta T}{\Delta t} = -\frac{g}{c_p}\frac{\Delta F}{\Delta p}$$

where T is temperature (K), t is time (s), g is gravitational acceleration (m s^{-2}), c_p is the specific heat of dry air (J K^{-1} kg^{-1}), F is the net all-wave flux (W m^{-2}), and p is the pressure (Pa). The gravitational acceleration is computed for each level from an empirical relationship derived for a standard atmosphere. Computations are begun at the top of the atmosphere. Layer heating/cooling rates are converted to degrees per day and are listed with the level that is their top. Therefore the surface level has a value of zero.

Some examples of the differences in downwelling surface shortwave and longwave fluxes for different numbers of streams (and hence the different solvers) are shown in Tables 1 and 2. The computations were done for the following conditions: no gaseous absorption, aerosol optical depth = 0.06, liquid cloud with a top at 550 mb, 10 μm effective radius, 0.2 g m^{-3} water content, and the mid-latitude summer profile.

τ:	**0**	**0.5**	**1**	**5**	**10**	**30**	**50**	**100**
			Solar Zenith = 0 degrees, Albedo = 0.1					
16-str:	1265.3	1239.7	1209.3	960.5	730.1	352.7	227.5	116.9
2-Toon:	1273.2	1348.3	1357.6	1032.4	750.1	345.9	219.7	111.2
% diff:	0.6	8.8	12.3	7.5	2.7	-1.9	-3.4	-4.9
			Solar Zenith = 0 degrees, Albedo = 0.8					
16-str:	1347.7	1362.4	1364.7	1270.9	1112.3	737.3	560.1	351.6
2-Toon:	1355.0	1473.2	1522.7	1381.8	1173.1	752.2	561.6	344.5
% diff:	0.5	8.1	11.6	8.7	5.5	2.0	0.3	-2.0
			Solar Zenith = 15 degrees, Albedo = 0.1					
16-str:	1219.6	1192.8	1161.3	911.7	690.3	333.5	215.1	110.6
2-Toon:	1226.8	1290.9	1294.2	975.7	708.7	326.9	207.6	105.1
% diff:	0.6	8.2	11.4	7.0	2.7	-2.0	-3.5	-4.9
			Solar Zenith = 15 degrees, Albedo = 0.8					
16-str:	1298.8	1310.6	1310.3	1206.6	1052.0	697.2	529.7	332.5
2-Toon:	1305.4	1410.3	1451.5	1306.0	1108.5	710.8	530.7	325.6
% diff:	0.5	7.6	10.8	8.2	5.4	2.0	0.2	-2.1
			Solar Zenith = 30 degrees, Albedo = 0.1					
16-str:	1085.6	1055.0	1020.2	772.4	579.4	279.9	180.6	92.8
2-Toon:	1091.0	1124.1	1111.8	817.9	593.9	274.0	174.0	88.1
% diff:	0.5	6.5	9.0	5.9	2.5	-2.1	-3.6	-5.1
			Solar Zenith = 30 degrees, Albedo = 0.8					
16-str:	1155.4	1158.6	1150.6	1022.6	883.5	585.2	444.7	279.2
2-Toon:	1160.1	1227.6	1246.6	1095.0	929.1	595.8	444.9	272.9
% diff:	0.4	6.0	8.3	7.1	5.2	1.8	0.0	-2.2
			Solar Zenith = 50 degrees, Albedo = 0.1					
16-str:	787.2	745.9	703.6	488.8	363.0	175.5	113.3	58.3
2-Toon:	789.4	762.7	728.0	512.4	372.1	171.7	109.1	55.2
% diff:	0.3	2.3	3.5	4.8	2.5	-2.1	-3.7	-5.2
			Solar Zenith = 50 degrees, Albedo = 0.8					
16-str:	836.2	817.7	792.6	647.9	554.1	367.2	279.2	175.3
2-Toon:	837.6	831.9	815.9	686.2	582.2	373.5	278.9	171.1
% diff:	0.2	1.7	2.9	5.9	5.1	1.7	-0.1	-2.4
			Solar Zenith = 80 degrees, Albedo = 0.1					
16-str:	178.3	129.6	113.4	75.2	56.1	27.2	17.6	9.1
2-Toon:	179.1	129.9	120.8	84.6	61.5	28.4	18.0	9.1
% diff:	0.4	0.2	6.5	12.4	9.7	4.2	2.3	0.4
			Solar Zenith = 80 degrees, Albedo = 0.8					
16-str:	187.7	141.9	127.9	100.0	85.8	57.2	43.5	27.4
2-Toon:	188.3	141.6	135.5	113.3	96.2	61.8	46.1	28.3
% diff:	0.3	-0.2	5.9	13.3	12.1	8.0	5.9	3.3

τ:	**0**	**0.5**	**1**	**5**	**10**	**30**	**50**	**100**
16-str:	20.6	127.3	187.2	292.3	302.1	318.3	334.7	379.1
2-Toon:	19.9	125.8	189.7	296.6	303.3	319.1	335.4	379.5
% diff:	-3.5	-1.2	1.4	1.4	0.4	0.3	0.2	0.1

The longwave fluxes computed with the 2-stream model are very accurate, with the largest error being for clear skies (under the test conditions). Shortwave fluxes generally have small errors **except for conditions of high sun (small solar zenith angle) and optically thin clouds**, where errors in the downwelling fluxes are 10-15%.

RADIANCES

Radiances are calculated at every atmospheric level, but reflectances (hereafter simply "albedos") and brightness temperatures are only computed for the TOA; i.e., for satellite simulations. The albedo is the ratio of the upwelling irradiance, approximated as the radiance times pi, to the top of the atmosphere solar flux. It will be weighted by the bandweights, if specified. An adjustment for solar zenith angle is made:

$$\alpha_{TOA} = \frac{\pi \sum_i L_i W_i}{\cos Z \sum_i S_i W_i}$$

where L_i is the radiance (W m^{-2} sr^{-1}) in *Streamer* band *i*, W_i is the user-specified band weight (set to 1 if not specified), *Z* is the solar zenith angle, and S_i is the solar flux (W m^{-2}). This formulation assumes that the radiance is isotropic, which is generally not the case, so in conditions of anisotropy the calculated albedo can exceed unity.

For brightness temperature calculations, the weighted integrated radiance is divided by the area under the response curve, which is based on the user-specified weights or, if no weights were given, it is the sum of the widths of all the bands (in that case the response for each band is 1.0). The central wavenumber used in the inversion of the Planck function when no weights file is specified is simply the midpoint of the wavelength range. This will be reasonably accurate if the response function is symmetrical. The general equation for brightness temperature *Tb* is

$$L^* = \frac{\sum_i L_i W_i}{\sum_i W_i \Delta\upsilon_i}$$

$$Tb = \frac{c_2 \upsilon}{\ln((c_1 \upsilon^3)/L^* + 1)}$$

where L* is the average radiance over band i, Δv_i is the width of a band in wavenumbers, c_1 and c_2 are Planck's constants, and v is the central wavenumber.

For satellite simulations, the angle of the emerging radiance, *theta*, needs to be adjusted. In a plane-parallel sense, this is the same as the satellite scan angle (or "look" angle or "view" angle or whatever you want to call it). It is close to, but not the same as, the scan angle for a **curved** earth, which is a function of the satellite altitude and the radius of the earth. In that case the scan angle θ_{scan} is

$$\theta_{scan} = \operatorname{asin}\left(R_{earth}\frac{\sin\theta_{zen}}{R_{earth} + H_{sat}}\right)$$

where θ_{zen} is the satellite sensor zenith angle (which is *theta* in *Streamer*), R_{earth} is the radius of the earth (6357 km), and H_{sat} is the satellite altitude. With the NOAA polar orbiters (e.g., the AVHRR), for example, which have a nominal height above the surface of 850 km, for a satellite zenith angle of 10 degrees the scan angle is 8.8 degrees; for a zenith angle of 50 degrees the scan angle is 42.5 degrees. The difference between these two angles also depends on the height of the object being viewed, though this effect is relatively small for observations within the troposphere and no adjustment is made in the model.

How does this impact the use of *Streamer* for satellite applications? In theory, *theta* should be calculated by inverting the above equation as

$$\theta = \operatorname{asin}\left((R_{earth} + H_{sat})\frac{\sin\theta_{scan}}{R_{earth}}\right).$$

So for the NOAA satellites, a scan angle of 10 degrees implies a *theta* of 11.4, while a scan angle of 50 degrees implies a *theta* of 60.3. *Streamer* will do the conversion automatically <u>if</u> a bandweights file is used and <u>if</u> the satellite altitude is given in the file. See *Input, Band Weights* in the *User's Guide* for details. In practice, uncertainties in the scattering properties of clouds, aerosols, and the surface probably result in much larger errors than differences between the satellite scan angle and *theta* in plane-parallel calculations.

3 GASEOUS ABSORPTION

Gas data were provided by S.-C. Tsay (*cf.*, Tsay et al., 1989). Absorption amounts are determined with the exponential-sum fitting of transmissions (ESFT) technique, which parameterizes the many absorption lines that may exist in a given spectral region. The basis of the ESFT method is that the transmission function *T(u)* for a given absorber amount *u* and for a given spectral interval is fit by a sum of exponentials *E(u)*:

$$T(u) \approx E(u) \equiv \sum_{i=1}^{M} a_i e^{-k_i u}$$

where M is the number of terms, k_i are the absorption coefficients, a_i are weights. The fluxes are computed for M monochromatic problems and are summed up with the weights a_i to give the spectrally integrated flux. See Wiscombe and Evans (1977) for more details.

Only four gases are present in *Streamer*: water vapor, carbon dioxide, ozone, and oxygen. Their presence/absence in each band is shown in the table below. Carbon dioxide and oxygen amounts cannot be input, so the only way to change their concentration is with the *frco2* and *fro2* input scaling variables. A carbon dioxide amount of 330 ppm was used in the development of the ESFT coefficients. Current values are in the range 350-360 ppm, so the carbon dioxide amount is scaled internally to an approximate value of 355 ppm. The absence of trace gases result in surface flux differences of a few W m^{-2}, determined using LOWTRAN.

Gases: 1=Water Vapor, 2=CO2, 3=O3, 4=O2

```
  Band    Gas     Band    Gas     Band    Gas     Band    Gas     Band    Gas
 (1/cm) 1 2 3 4 (1/cm) 1 2 3 4 (1/cm) 1 2 3 4 (1/cm) 1 2 3 4 (1/cm) 1 2 3 4
Longwave:
    20: X - - -    40: X - - -    60: X - - -    80: X - - -   100: X - - -
   120: X - - -   140: X - - -   160: X - - -   180: X - - -   200: X - - -
   220: X - - -   240: X - - -   260: X - - -   280: X - - -   300: X - - -
   320: X - - -   340: X - - -   360: X - - -   380: X - - -   400: X - - -
   420: X - - -   440: X - - -   460: X - - -   480: X - - -   500: X X - -
   520: X X - -   540: X X - -   560: X X - -   580: X X - -   600: X X - -
   620: X X - -   640: X X - -   660: X X - -   680: X X - -   700: X X - -
   720: X X - -   740: X X - -   760: X X - -   780: X X - -   800: X X - -
   820: X X - -   840: X - - -   860: X - - -   880: X - - -   900: X - X -
   920: X - X -   940: X - X -   960: X - X -   980: X - X -  1000: X - X -
  1020: X - X -  1040: X - X -  1060: X - X -  1080: X - X -  1100: X - X -
  1120: X - X -  1140: X - X -  1160: X - X -  1180: X - X -  1200: X - X -
  1220: X - X -  1240: X - X -  1260: X - X -  1280: X - - -  1300: X - - -
  1320: X - - -  1340: X - - -  1360: X - - -  1380: X - - -  1400: X - - -
  1420: X - - -  1440: X - - -  1460: X - - -  1480: X - - -  1500: X - - -
  1520: X - - -  1540: X - - -  1560: X - - -  1580: X - - -  1600: X - - -
  1620: X - - -  1640: X - - -  1660: X - - -  1680: X - - -  1700: X - - -
  1720: X - - -  1740: X - - -  1760: X - - -  1780: X - - -  1800: X - - -
  1820: X - - -  1840: X - - -  1860: X - - -  1880: X - - -  1900: X - - -
  1920: X - - -  1940: X - - -  1960: X - - -  1980: X - - -  2000: X - - -
  2080: X - - -  2160: X - - -  2240: X - - -  2320: X - - -  2400: X - - -

Shortwave:
  2500: X - - -  2920: X X - -  3440: X - - -  4200: X - - -  4700: X X - -
  6080: - X - -  6520: X X - -  7840: - - - -  8400: X - - -  9120: - - - -
 10000: X - - - 11540: X - - - 12820: - - - X 13300: X - - - 14500: - - X -
 15620: - - X - 17540: - - X - 19240: - - X - 20840: - - - - 22720: - - - -
 25000: - - - - 27780: - - X - 30300: - - X - 33340: - - X -
```

4 STANDARD PROFILES

Profiles are based on data in Ellingson et al. (1991) except for the Arctic profiles of temperature and humidity, which are based on Arctic Ocean coastal and drifting station data. The altitudes for all standard profiles are given in the table below. Standard profile characteristics are shown in Figures 15-1 through 15-4.

Standard Altitudes (km)

100.0000	70.0000	50.0000	45.0000	40.0000	35.0000	30.0000	25.0000
20.0000	15.0000	14.0000	13.0000	12.0000	11.0000	10.0000	9.0000
8.0000	7.0000	6.0000	5.0000	4.0000	3.0000	2.0000	1.0000
0.0000							

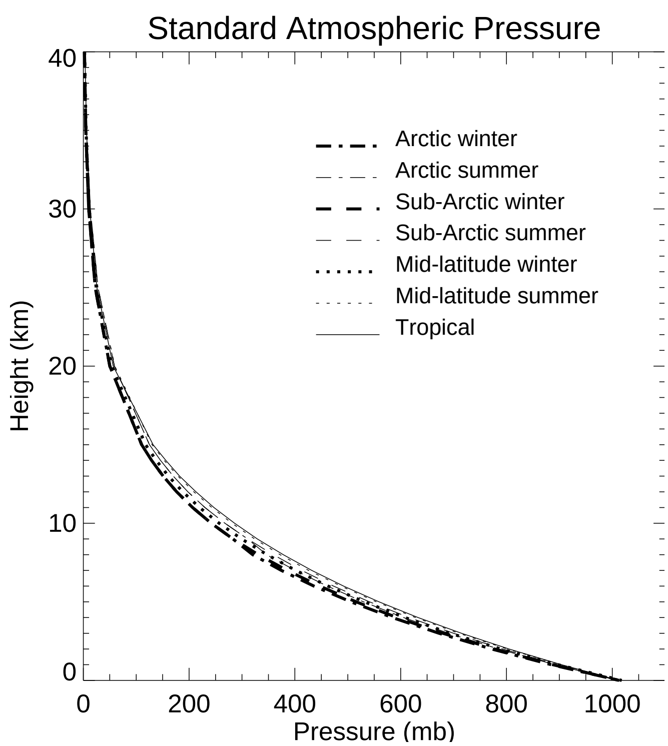

Fig. 4-1. Vertical profiles of pressure.

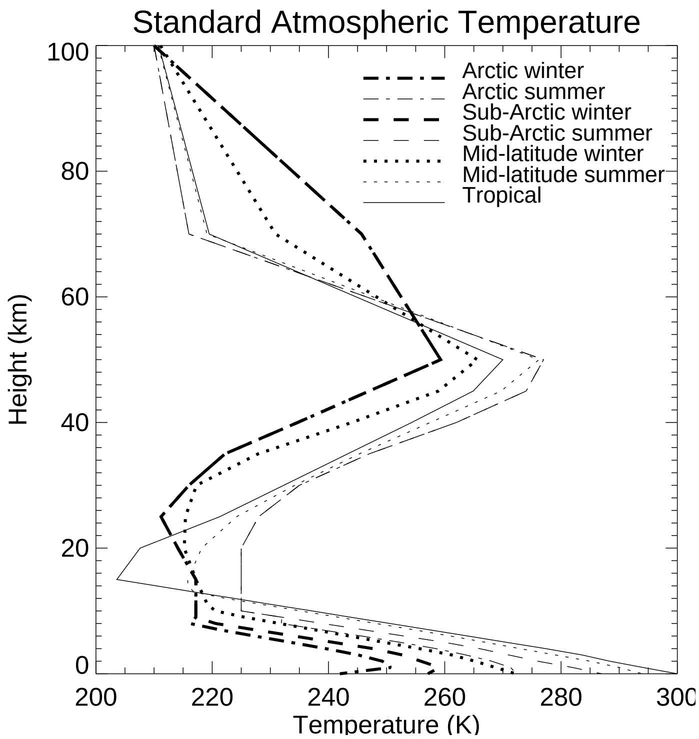

Fig. 4-2. Vertical profiles of temperature.

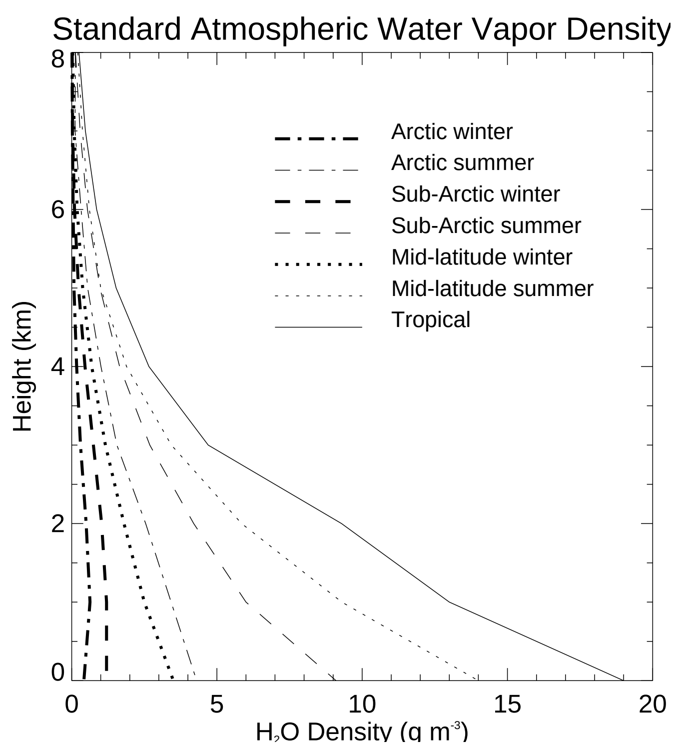

Fig. 4-3. Vertical profiles of water vapor.

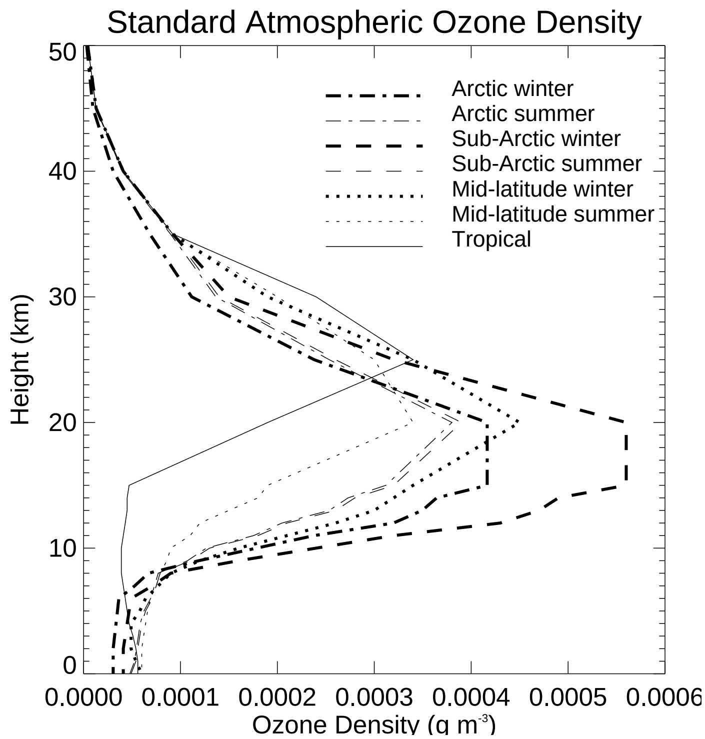

Fig. 4-4. Vertical profiles of ozone.

The "standard" Arctic summer and winter profiles were constructed using radiosonde data from the Historical Arctic Rawinsonde Archive (HARA; http://www.nsidc.colorado.edu). Temperature and humidity profiles from the radiosonde data were averaged over all locations from 80N to the pole. Winter means December - February; summer is June - August. Temperature and humidity above 300 mb were filled in with values from the standard subarctic summer and winter profiles. Altitudes were calculated with the hypsometric equation. Total column ozone amounts were taken from the ISCCP C2 data, and were distributed vertically according to the subarctic summer and winter profiles. In other words, the total column ozone amounts are specific to the Arctic, but the vertical distribution (shape) follows the subarctic profiles.

5 AEROSOLS

Aerosol amounts can be distributed vertically either by a user-supplied profile or one of the internal "standard" profiles of the extinction coefficient. Four profiles are available that are combinations of two tropospheric and two stratospheric loadings:

1. Background tropospheric aerosols, 50 km visibility, and background stratospheric amounts (B50,T50, SBK in Figure 16-1).
2. High tropospheric loadings with 5 km visibility from 0-2 km vertically, 23 km visibility between 2 and 10 km; background stratospheric amounts (B05, T23, SBK).
3. Background tropospheric as in #1, high volcanic stratospheric aerosols (B50, T50, SHV).
4. High tropospheric loadings as in #2, high volcanic stratospheric amounts (B05, T23, SHV).

These profiles are shown in Figure 16-1. The data are taken from LOWTRAN-7. Total aerosol optical depths for these profiles were somewhat arbitrarily chosen as 1: 0.08, 2: 0.66, 3: 0.29, and 4: 0.86.

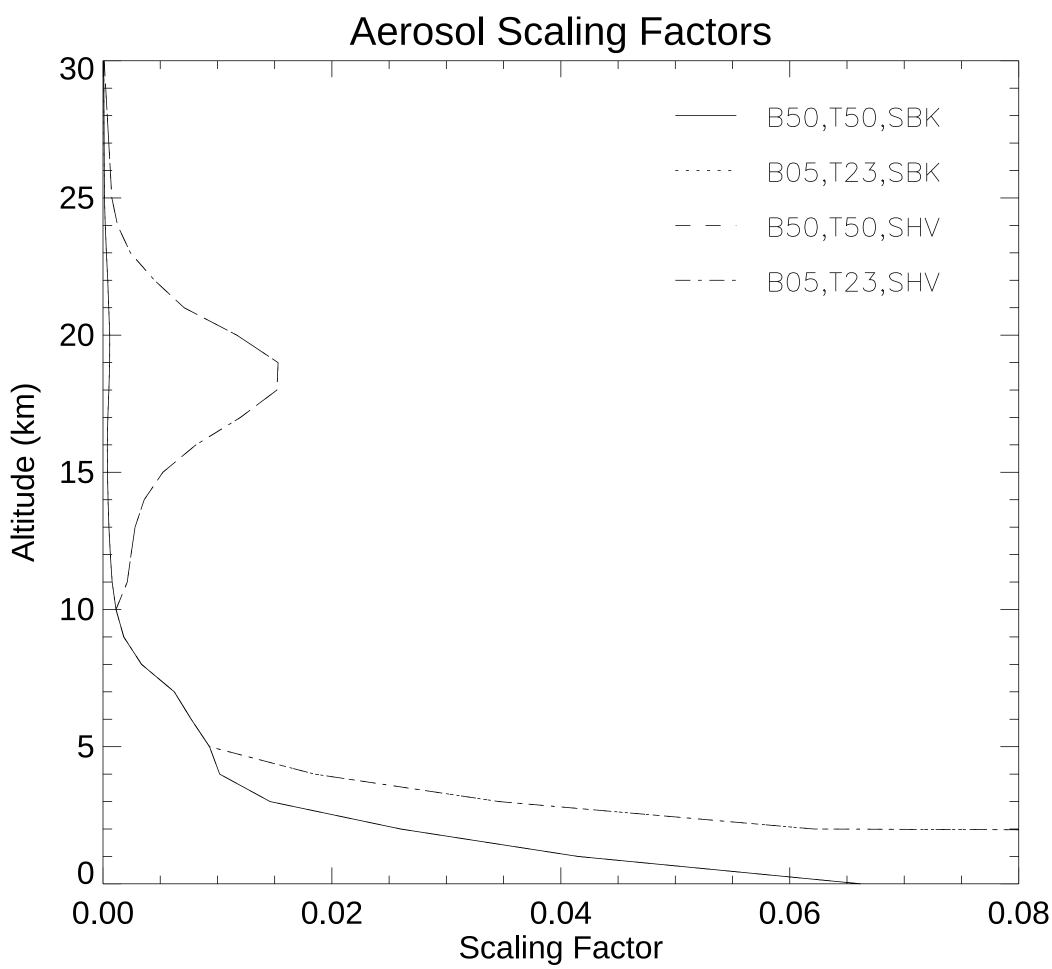

Fig. 5-1. Vertical profiles of the aerosol scaling factors in *Streamer.*

Aerosol optical properties are taken from LOWTRAN-7 (also given in Shettle and Fenn, 1979) for the tropospheric, rural, urban, and maritime models. Arctic haze optical properties are from Blanchet and List (1983) for the shortwave portion of the spectrum. For the longwave portion the optical properties of the tropospheric model are used if Arctic haze is selected. The optical properties of smoke were calculated with the Mie code of Tsay and Stephens (1990) as a combination of soluble particles with soot and sulfuric acid, an effective radius of approximately 0.05 microns, and a number density of 500 cm^{-3} (B. Baum, personal communication, 2000). The optical properties of the different aerosol models are shown in Figures 16-2 through 16-4 for a relative humidity of 70%.

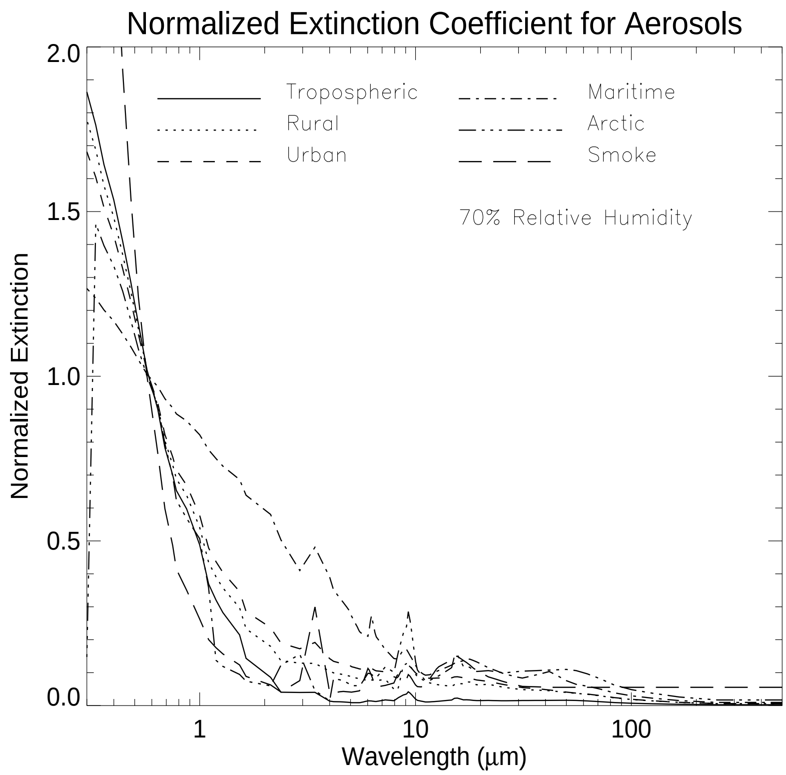

Fig. 5-2. Normalized extinction coefficient of the tropospheric, urban, rural, and maritime aerosol models. The volume extinction coefficient is normalized such that the value at 0.55 µm is 1.0.

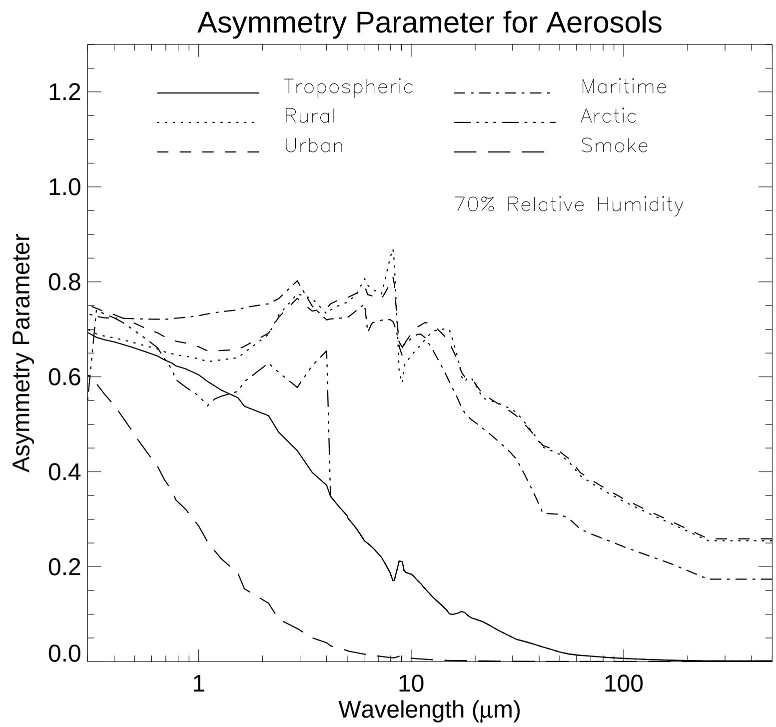

Fig. 5-3. Asymmetry parameter of the aerosol models.

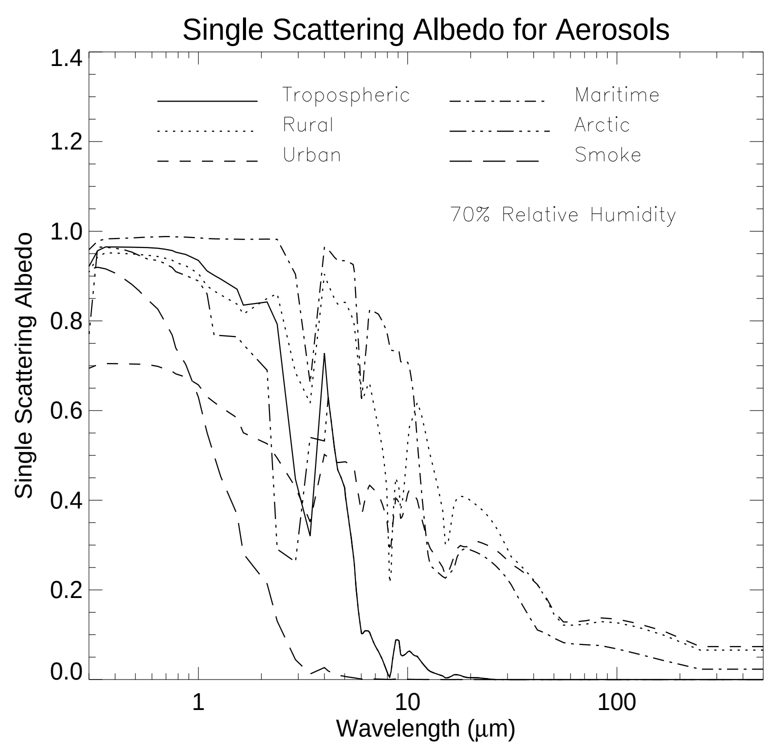

Fig. 5-4. Single scattering albedo of the aerosol models.

6 CLOUD PROPERTIES

CLOUD OPTICAL PROPERTIES

Cloud optical properties are based on parameterization schemes from three different sources. For water clouds, the data are taken from Hu and Stamnes (1993). Effective radii range from 2.5 to 60 microns and are given for 293 wavelengths throughout the shortwave and longwave portions of the spectrum. Longwave ice cloud optical properties are based on Mie calculations using spherical particles for 132 wavelengths. This parameterization is unpublished but follows the methodology of Hu and Stamnes almost exactly. It is important to point out that using spherical particles in the determination of ice cloud optical properties may not be realistic, since ice crystals may take on a variety of shapes (cf, Takano and Liou, 1989; Schmidt et al., 1995). However, no parameterization using other shapes (e.g., hexagons) across the entire longwave range at a sufficiently high spectral resolution is currently available.

For ice clouds in the shortwave there are parameterizations for a variety of ice shapes or "habits" as shown in Figure 17-1. Optical properties of seven habits have been parameterizaed by Key et al. (2001). That work extends the parameterizations of Fu and Liou (1993) and Ebert and Curry (1992) for randomly oriented hexagonal crystals. The spherical particle model based on Mie calculations described above is also available.

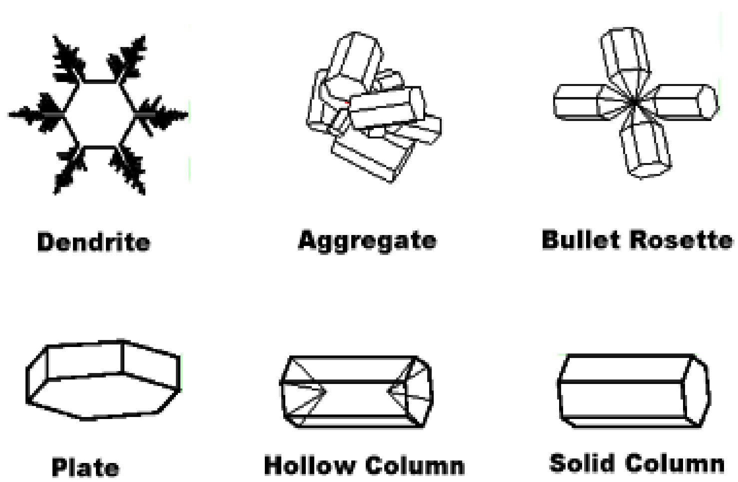

Fig. 6-1. Idealized ice particle shapes or "habits". Spheres are not shown. (Courtesy P. Yang)

Water (liquid) and ice cloud parameterizations are based on the empirical relationships between the particle effective radius, water content, and extinction, single scatter albedo, and the asymmetry parameter. For liquid clouds at all wavelengths and the spherical particle ice clouds model, the forms of the parameterizations are:

$$\frac{\beta_{ext}}{WC} = a_1 r_e^{b_1} + c_1$$

$$\omega = a_2 r_e^{b_2} + c_2$$

$$g = a_3 r_e^{b_3} + c_3$$

where β_{ext} is the volume extinction coefficient, *WC* is the liquid/ice water content, ω is the single scatter albedo, *g* is the asymmetry parameter, and *a*, *b*, and *c* are coefficients determined through a least squares nonlinear regression. The effective radius, which in *Streamer* applies to liquid droplets and ice particles in the longwave (only), is defined as

$$r_e = \frac{\int_0^\infty r^3 n(r) dr}{\int_0^\infty r^2 n(r) dr} .$$

For nonspherical ice particles such as plates, hexagonal crystals, bullet rosettes, aggregates, and dendrites, the parameterization is based on ray tracing calculations of randomly oriented particles. The parameterization uses an effective "radius" defined as

$$R_e = \frac{3}{4} \frac{\int_{L_{min}}^{L_{max}} V(L) n(L) dL}{\int_{L_{min}}^{L_{max}} A(L) n(L) dL}$$

where *L* is the maximum dimension of an ice crystal, *V* is the volume of the crystal, A is the projected area, and *n(L)* is the size distribution. The optical properties are

$$\frac{\beta_{ext}}{WC} = \sum_{n=0}^{3} a_n \frac{1}{R_e^n}$$

$$\omega = \sum_{n=0}^{3} b_n R_e^n$$

$$g = \sum_{n=0}^{3} c_n R_e^n$$

where *a*, *b*, and *c* are empirical coefficients determined through regression. Ice water content is calculated as $V\rho$, where ρ is the density of ice. A value of ρ= 0.9167 g cm^{-3} was used.

Water cloud and spherical particle ice cloud optical properties were determined at a relatively high spectral resolution and then averaged over *Streamer* bands. For nonspherical ice particles the parameterization spectral bands match *Streamer*'s bands. **NOTE: At present this parameterization has only been developed for the shortwave portion of the spectrum. For the longwave, the spherical ice particle model is used.** The optical properties are shown in Figures 17-2 - 17-7.

The asymmetry parameter is commonly used with the Henyey-Greenstein (HG) function as an approximation to the scattering phase function. The HG function is defined as

$$P_{\mathrm{HG}}(\theta;g) = \frac{1-g^2}{(1+g^2-2g\cos\theta)^{3/2}} .$$

The function represents forward scattering reasonably well but it does not capture backscattering behavior. This problem can be remedied through the use of the double Henyey-Greenstein function:

$$P_{\mathrm{dHG}}(\theta) = fP_{\mathrm{HG}}(\theta;g_1) + (1-f)P_{\mathrm{HG}}(\theta;g_2)$$

where g_2 can be assigned a negative value to account for a backscattering peak and *f* is a positive fraction in the range [0,1] [cf., Hu et al., 2000]. The double Henyey-Greenstein function is only used with more than two-streams, and (at present) only for ice clouds in the shortwave.

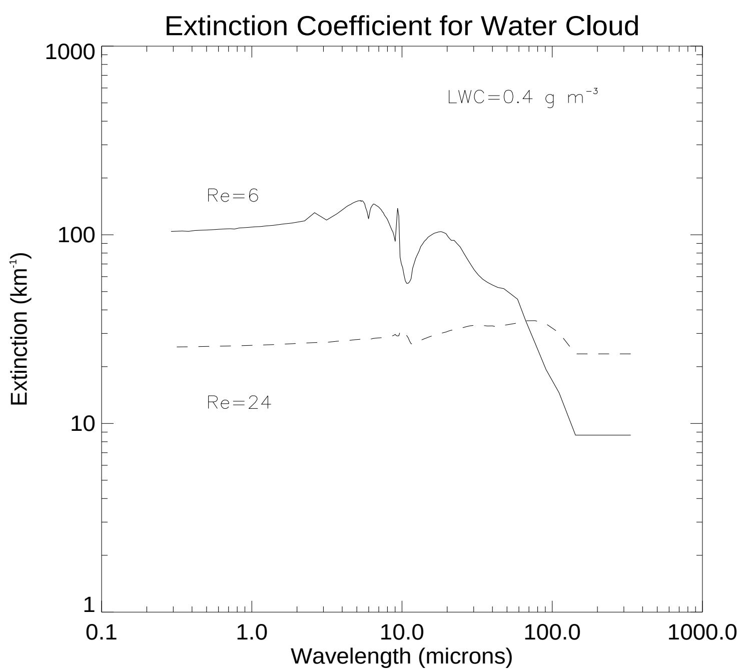

Fig. 6-2. Extinction coefficients of water cloud for the indicated effective radii and liquid water concentrations.

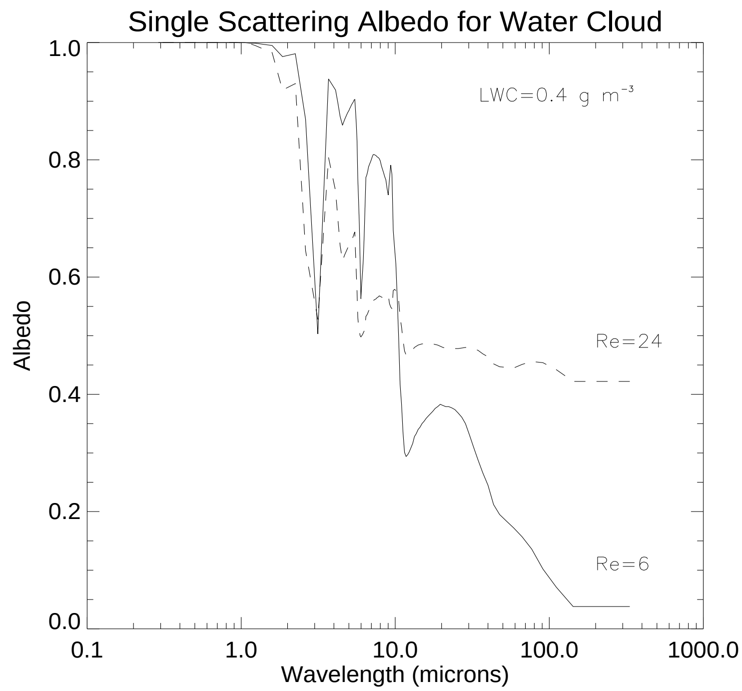

Fig. 6-3. Single scattering albedo of water cloud for the indicated effective radii and liquid water concentrations.

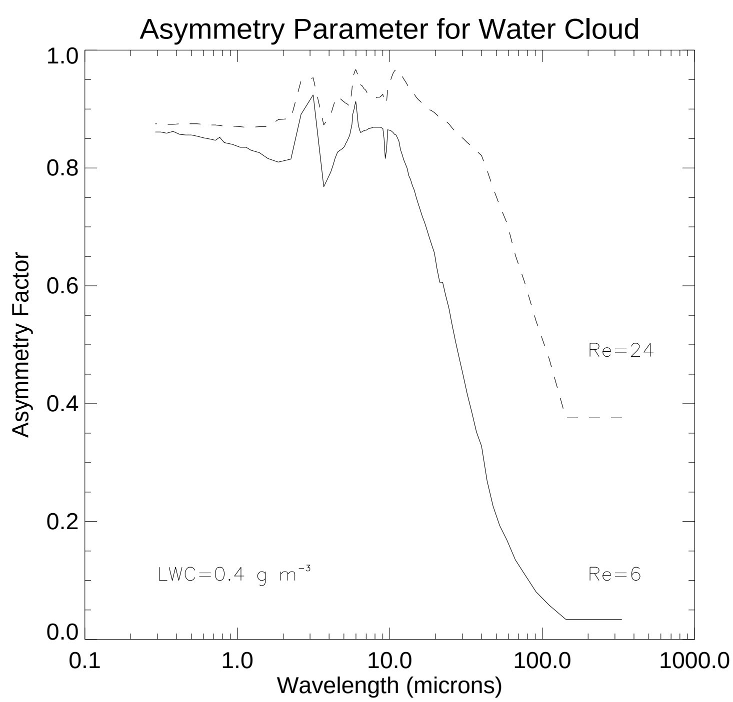

Fig. 6-4. Asymmetry parameter of water cloud for the indicated effective radii and liquid water concentrations.

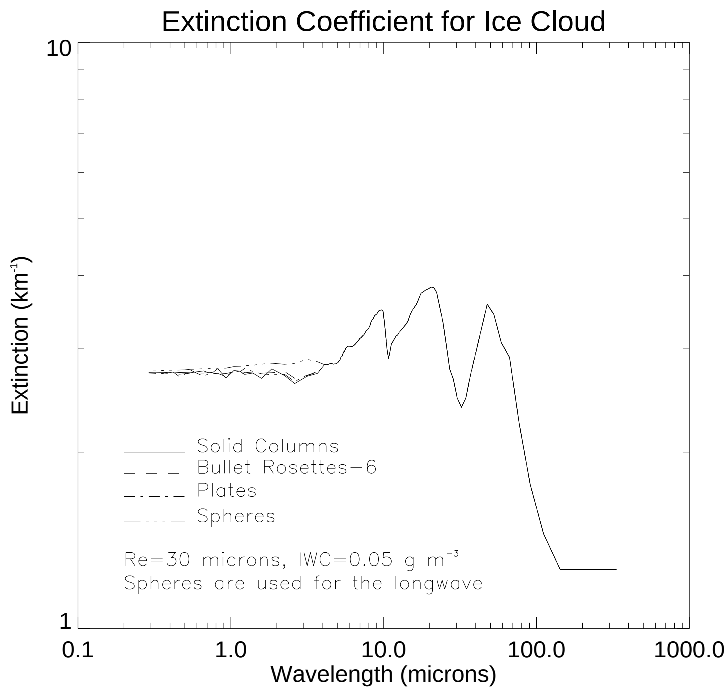

Fig. 6-5. Extinction coefficients of ice cloud for the indicated effective radius and ice water concentration.

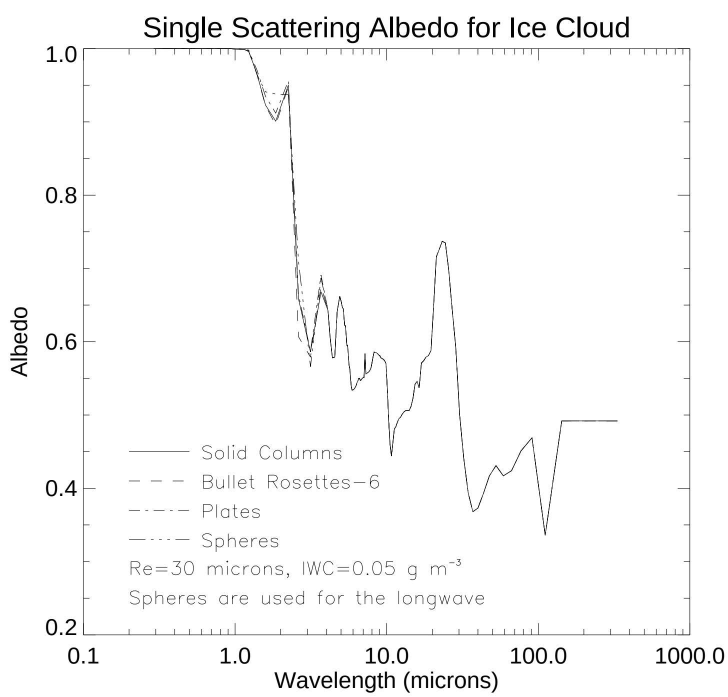

Fig. 6-6. Single scattering albedo of ice cloud for the indicated effective radius and ice water concentration.

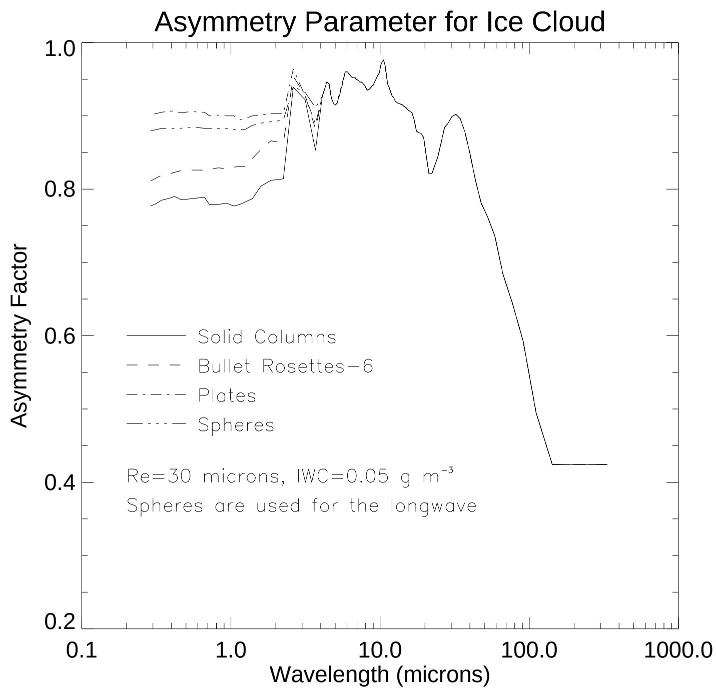

Fig. 6-7. Asymmetry parameter of ice cloud for the indicated effective radius and ice water concentration.

For nonspherical ice particles the relationship between effective "radius" and other measures of particle size is not straightforward. As defined above, the effective radius is a function of the volume to area projected ratio. Therefore, a particle that is large in one dimension but small in the other may have a small effective radius. For example, dendrites are broad but thin, so the projected area is large (for the orientation used here) and the effective radius is small. Figure 17-8 illustrates the relationship between the effective radius and maximum dimension over 30 size distributions for each particle habit Mixed-phase cloud optical properties are a weighted average of the liquid and ice portions. Following Cess (1985), these are:

$$\beta_{ext} = \beta_{liq} + \beta_{ice}$$

$$\omega = \frac{\omega_{liq}\beta_{liq} + \omega_{ice}\beta_{ice}}{\beta_{liq} + \beta_{ice}}$$

$$g = \frac{g_{liq}\omega_{liq}\beta_{liq} + g_{ice}\omega_{ice}\beta_{ice}}{\omega_{liq}\beta_{liq} + \omega_{ice}\beta_{ice}}$$

where the subscript *liq* is for the liquid portion of the cloud and *ice* is for the ice portion. The methodology is the same for combining the optical properties of two ice particle habits. The g_2 and f parameters of the double Henyey-Greenstein function can be determined for mixtures in the same way as g above. For mixtures that include a liquid portion the parameters g_2 and f for the droplets are assumed to be 0 and 1, respectively.

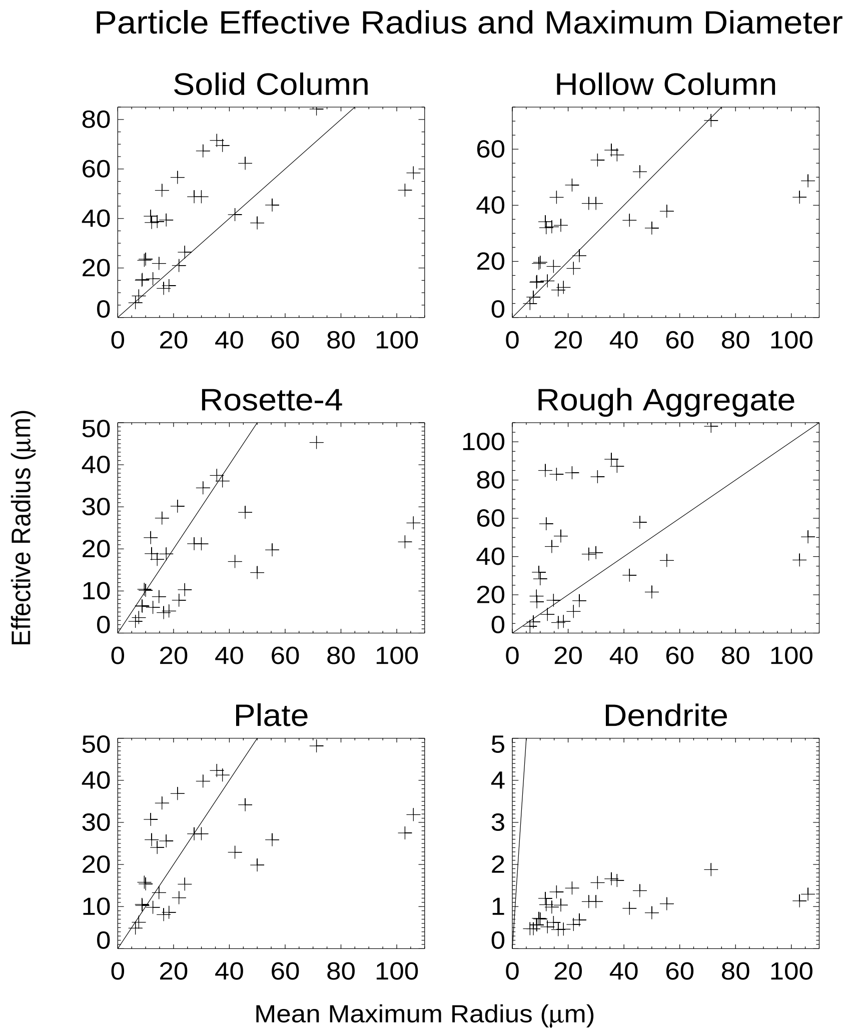

Fig. 6-8. Relationship between effective radius and the maximum dimension of nonspherical ice particles. Each plus sign represents the values for a different size distribution.

CLOUD THICKNESS AND WATER CONTENT

If cloud geometrical thickness z (mb or km) is not input then it is calculated from the visible optical thickness τ from

$$\tau = z\beta_{ext}$$

where the volume extinction coefficient β_{ext} is determined as in (17.1), (17.6), and (17.9) with the effective radius and water content. If the geometrical thickness is given but the optical thickness is not, then τ is determined from (17.12).

When both geometrical and optical thickness are given, water content is computed. This is accomplished by obtaining the the right-hand side of (17.1) or (17.6) from the effective radius, then solving for water content with the extinction computed from (17.12).

Cloud water path, which is only available as an output variable, is calculated from the cloud water content and geometrical thickness as $WP = z\ WC$.

COMBINING AEROSOL AND CLOUD OPTICAL PROPERTIES

Aerosol and cloud optical properties are combined when they both exist in a given layer. Additionally, aerosol and cloud optical properties are combined with Rayleigh scattering where appropriate. The single scattering albedo for a given layer i is

$$\omega(i) = \frac{\tau_{sca,\,cld}(i) + \tau_{sca,\,aer}(i) + \tau_{sca,\,ray}(i)}{\tau_{ext}(i)}$$

where $\tau_{sca,*}$ is the scattering optical depth for cloud (subscript *cld*), aerosols (subscript *aer*), and Rayleigh scattering (subscript *ray*). τ_{ext} is the total extinction optical depth for the layer defined by

$$\tau_{ext}(i) = \tau_{ext,\,cld}(i) + \tau_{ext,\,aer}(i) + \tau_{ext,\,ray}(i)$$

where $\tau_{ext,*}$ are the extinction optical depths for cloud, aerosols, and Rayleigh scattering. The extinction optical depth is the volume extinction coefficient times the layer thickness Δz; the scattering optical depth is the single scattering albedos times the extinction optical depth. For example, the extinction and scattering optical depths for cloud are computed as:

$$\tau_{ext,\,cld} = \beta_{ext,\,cld}\Delta z$$

$$\tau_{sca,\,cld} = \omega_{cld}\tau_{ext,\,cld}$$

The corresponding values for aerosols and Rayleigh scattering are defined similarly. For Rayleigh scattering, the single scattering albedo is unity so the scattering and extinction optical depths are equal.

The asymmetry parameter for a layer is the weighted, normalized sum of the products of the scattering optical depths and the asymmetry parameters of the cloud and aerosol:

$$g(i) = \frac{\tau_{sca,\,cld}(i)g_{cld}(i) + \tau_{sca,\,aer}(i)g_{aer}(i)}{\tau_{sca,\,cld}(i) + \tau_{sca,\,aer}(i) + \tau_{sca,\,ray}(i)}$$

The asymmetry parameter as defined above is used with the two-stream solver (Toon et al., 1989). For calculations with DISORT (Stamnes et al., 1988) the Legendre expansion of the phase function is used. The Legendre coefficients for a layer are weighted sums of the coefficients for cloud and aerosol, calculated in the same manner as the asymmetry parameter.

7 SURFACE REFLECTANCE

SPECTRAL ALBEDO MODELS

Figure 18-1 shows the surface albedo models are available in *Streamer.* These are based on either modeled or observed data in the literature. Sand data are from Tanre et al. (1986); meltpond and bareice albedos are from Grenfell and Maykut (1977); open sea water data are based on Brieglieb et al. (1985); freshwater (not shown) albedos are from Fresnel calculations; and snow data are computed using a 4-stream model (courtesy A. Schweiger). Spectral albedos for grass, dry grass, deciduous forest, and coniferous forest were taken from the ASTER Spectral Library v1.0 CD (1988, California Institute of Technology). The ASTER spectral library is currently made up of three other spectral libraries: the Jet Propulsion Laboratory (JPL) Spectral Library, the Johns Hopkins University (JHU) Spectral Library, and the United States Geological Survey (USGS - Reston) Spectral Library. The four vegetation types are based on the JHU data. Generic vegetation is an average of grass, dry grass, deciduous forest, and coniferous forest.

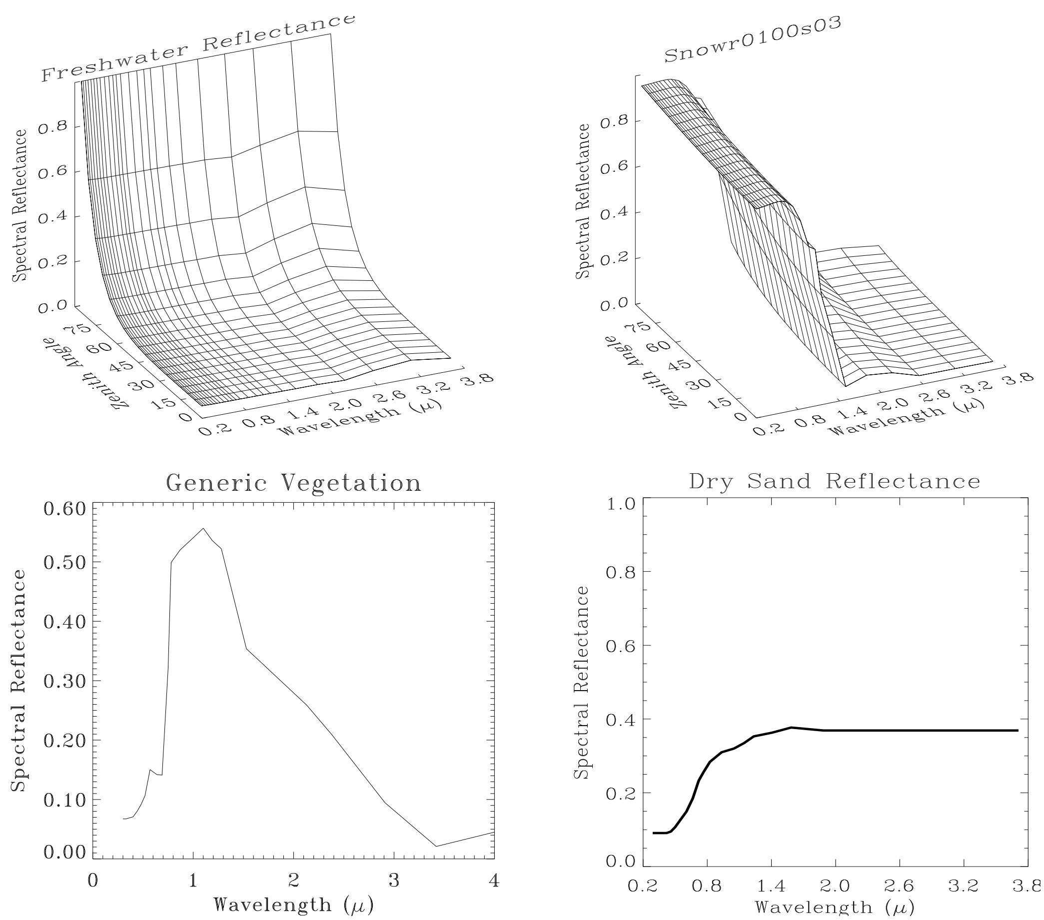

Fig. 7-1. Spectral albedo/reflectance “models” available in *Streamer.*

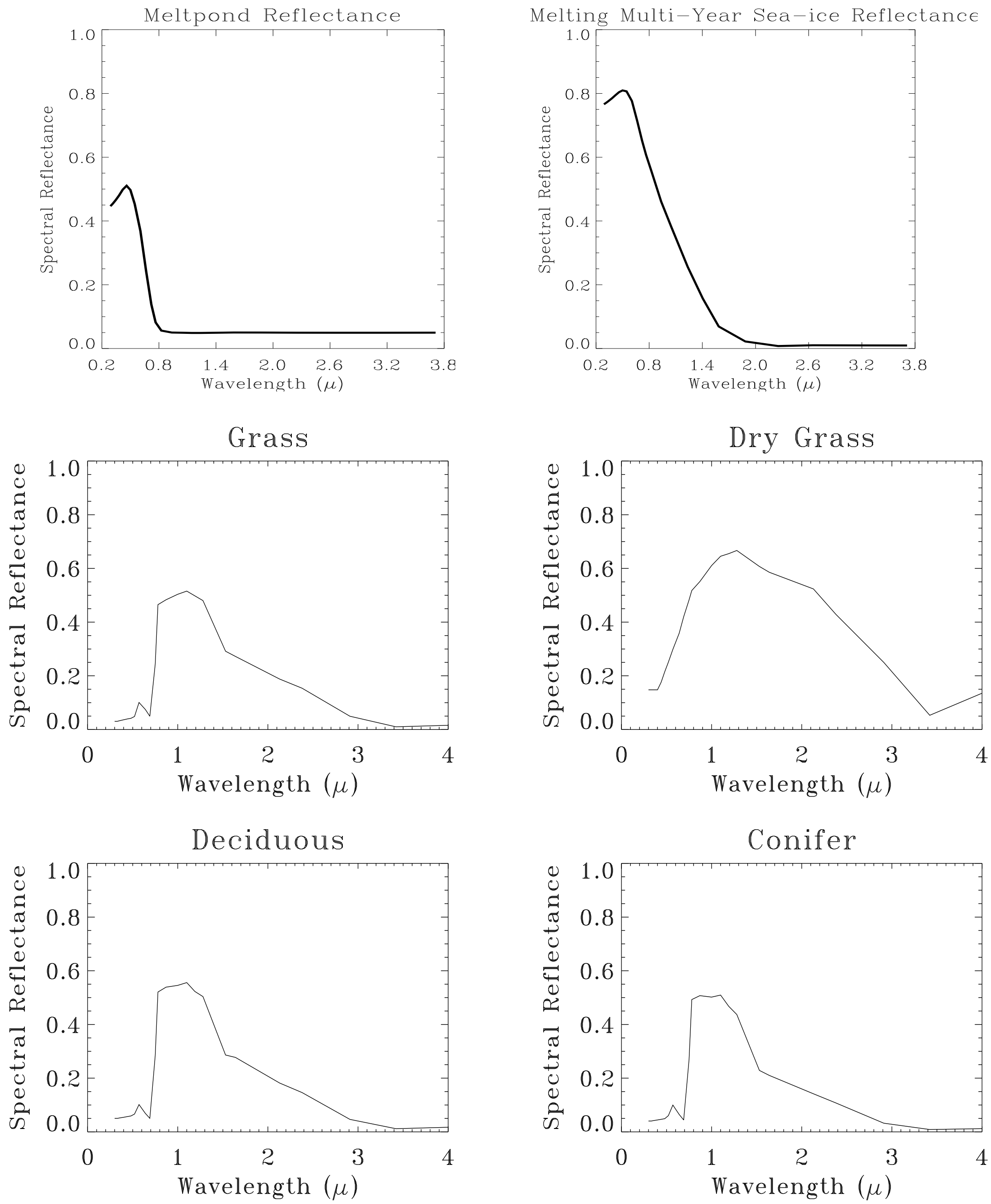

Figure 18-1, cont.

USER-SPECIFIED BIDIRECTIONAL REFLECTANCE FUNCTIONS

To utilize a user-defined bidirectionally reflecting surface the bidirectional reflectance distribution function (BRDF) values for the appropriate ranges of wavelength and viewing/illumination geometries are given in a file. The BRDF is defined as

$$L(\mu, \phi) = \int_0^{2\pi}\int_0^1 \gamma(\mu, \mu_p', |\phi - \phi_p'|)L(\mu_p', \phi_p')\mu_p' d\mu_p' d\phi_p'$$

where $L(\mu_p,\phi_p)$ is the downwelling radiance, $L(\mu,\phi)$ is the upwelling (reflected) radiance, μ is the cosine of the angle of reflection, ϕ is the corresponding azimuth angle, μ_p is the cosine of the incidence angle, ϕ_p is the corresponding azimuth angle (radians), $|\phi - \phi_p|$ is the relative azimuth angle (radians), and γ is the surface bidirectional reflectance (sr^{-1}). The integral of the BRDF over all view angles equals the surface albedo.

For a direct beam with no atmosphere the above relationship can be expressed as

$$\gamma(\mu, \mu_p, |\phi - \phi_p|) = \frac{L(\mu, \phi)}{E}$$

where E is the the incident flux. In DISORT the integral in (18.1) is multiplied by $1/\pi$ so the right-hand side of (18.2) is multiplied by π. This adjustment is done internally in *Streamer.* Use the definitions above when supplying BRDF values.

While not used directly in Streamer, it is useful to define the anisotropic reflectance factor (ARF). The ARF is proportional to the ratio of the upwelling radiance to the upwelling flux:

$$\xi(\mu, \mu_p, |\phi - \phi_p|) = \frac{\pi L(\mu, \phi)}{M} = \frac{\pi}{A}\gamma(\mu, \mu_p, |\phi - \phi_p|)$$

where A is the albedo and M is the reflected flux. The ARF therefore relates the radiance from a surface to that from a Lambertian surface with the same albedo. The integral of the ARF over all view angles equals π.

BIDIRECTIONAL REFLECTANCE MODELS

Streamer provides BRDF models (parameterizations) that can be used for a variety of surface types.

HAPKE MODEL

The model of Hapke (1981), modified for use with DISORT, is

$$\gamma_{hapke} = \frac{\omega}{4}\frac{1}{\mu + \mu_p}\{[1 + B(g)]P(g) + H(\mu)H(\mu_p) - 1\}$$

where μ_p is cosine of incidence angle, μ is cosine of view angle, g is phase (scattering) angle, ω is the single scattering albedo, $B(g)$ is a backscattering function, $p(g)$ is the phase function, and $H(x)$ is a function that accounts for multiple scattering. The modification of Hapke's model for DISORT involved multiplication by pi and division by μ_p. The scattering angle is

$$\cos(g) = \mu\mu_p + (1 - \mu^2)^{0.5}(1 - \mu_p^{\ 2})^{0.5}\cos\phi'$$

where ϕ' is the relative azimuth angle. The backscattering function ranges from -1 to +1 and is defined as

$$B(g) = \frac{B0}{1 + \left(\frac{1}{h}\right)\tan\left(\frac{g}{2}\right)}$$

where h is the width of the hot spot. The magnitude or amplitude of the hot spot is

$$B0 = \frac{S}{\omega p(0)}$$

which is controlled by the relative value of the parameter S. The phase function $p(g)$ employed here is the Henyey-Greenstein function:

$$p(g) = \frac{(1 - \Theta^2)}{(1 + \Theta^2 + 2\Theta\cos g)^{3/2}}$$

where Θ is the asymmetry factor ranging from -1 to 1. (Notes: This is somewhat confusing given that g is commonly used as the asymmetry factor! This version of the Henyey-Greenstein function varies from some traditional definitions by the addition rather than substraction of the last term in the denominator.) Finally, $H(x)$ accounts for multiple scattering and is defined by

$$H(x) = \frac{1+2x}{1+2x(1-\omega)^{0.5}}$$

The parameters of the Hapke model (*brdftype*=1) that must be specified are ω, θ, *S*, and *h*.

RAHMAN MODEL

Rahman et al. (1993) developed a three-parameter semi-empirical model that describes the bidirectional reflectance of arbitrary natural surfaces:

$$\gamma_{rahman} = \rho_0 \frac{\mu^{k-1}\mu_p^{\;k-1}}{(\mu+\mu_p)^{1-k}} F(g)[1+R(G)]$$

where ρ_0 and k are empirical surface parameters. The function F(g) is the Henyey-Greenstein function:

$$F(g) = \frac{(1-\Theta^2)}{[1+\Theta^2-2\Theta\cos(\pi-g)]^{3/2}}$$

where g is the phase angle and Θ controls the relative amount of foreward (0 <= Θ <= +1) and backward scattering (-1 <= Θ <= 0). Note the difference between this version of the Henyey-Greenstein function and that used by Hapke above. The hot-spot effect is approximated by

$$R(G) = 1 + \frac{1-\rho_0}{1+G}$$

where G is defined in Rahman et al. (1993).

The coefficient ρ_0 characterizes the intensity of the reflectance of the surface cover, but it should not be taken as a single-scattering albedo or as a normalized reflectance. It is arbitrary, and the only constraint on it is that it is zero or greater, and that the integral of the BRDF over all angles equals the albedo, which cannot exceed 1. **Important**: It is very easy to make this coefficient too large, resulting in an physically unrealistic albedo. Typical values for vegetation are in the range 0-0.5. See Rahman et al. (1993) for guidance. The parameter *k* controls the level of anisotropy of the surface. When k = 1 the resulting anisotropy comes solely from *F(g)* and the hot spot effect.

The parameters of the Rahman model (*brdftype*=2) that must be specified are ρ_0, *k*, and Θ.

ROUJEAN MODEL

Roujean et al. (1992) developed a BRDF model using a semiempirical approach applicable to heterogeneous surface. It considers the surface reflectance to be the sum of two main processes: a diffuse reflection component that accouts for the geometrical structure of opaque reflectors on the surface and a volume scattering contribution:

$$\gamma_{roujean} = a\gamma_{geom} + (1 - a)\gamma_{vol}$$

where a is an empirical coefficient that characterizes the relative weight of the geometric and volume components (γ_{geom} and γ_{vol}) in the bidirectional signature. The model specified above may be written as

$$\gamma_{roujean} = k_0 + k_1 f_1 + k_2 f_2$$

where γ, f_1, and f_2 are all a function of viewing and illumination geometry as defined in Roujean et al. (1992), k_0 represents the BRDF for viewing and illumination zenith angles of 0, k_1 is proportional to the height and length of surface protrusions, and k_2 is related to the reflectance and area of facets.

This semiempirical model was developed primarily for vegetated surfaces and bare soils. Some values for the parameters are given in the table below, as presented in Roujean et al. (1992, their Table 1).

Table 1: Roujean et al. (1992) parameter values for various surfaces.

	Visible Band			Near-Infrared Band		
Surface	k_0	k_1	k_2	k_0	k_1	k_2
Plowed field	0.243	0.073	0.642	0.288	0.085	0.748
Annual grass	0.349	0.044	0.377	0.452	0.053	0.503
Hard wheat	0.273	0.052	0.269	0.373	0.033	0.802
Steppe	0.266	0.050	0.059	0.356	0.056	0.217
Corn	0.084	0.006	0.001	0.272	0.000	0.285
Pine forest	0.037	0.000	0.133	0.282	0.017	0.243
Deciduous forest	0.030	0.000	0.087	0.400	0.040	0.295
Soybean	0.032	0.000	0.084	0.528	0.001	0.460

The parameters of the Roujean model (*brdftype*=3) that must be specified are k_0, k_1, and k_2.

Default BRDF Models for Various Surface Types

Default values of parameters for the BRDF models described above are available for various surface types. This allows for the use of generic surface BRDFs. This functionality is enabled when the *ALBTYPE* option is set to 5. The currently available surface types with this option are:

Generic vegetation - Actually for clover. Uses the Hapke model with ω=0.101, θ=-0.263, S=0.589, and h=0.046. From Pinty and Verstraete (1991).

Snow - Uses the Hapke model with ω=0.99, θ=0.6, S=0.0, and h=0.995. Based on Domingue et al. (1997) and Verbiscer and Veverka (1990).

8 SOLAR FLUXES

TOA solar fluxes used in *Streamer*, given below, are compiled from MODTRAN3, where fluxes for all wavenumbers (cm^{-1}) are summed over the *Streamer* bands. The total flux in the shortwave spectrum (0.28 - 4.0 μm) is 1354.2 W m^{-2}. These are based on the mean Earth-Sun distance, which is adjusted for actual Earth-Sun distance based on the day of the year.

	Flux (W m^{-2})				
Band	+0	+1	+2	+3	+4
106:	6.79596	11.25329	22.57683	19.13139	72.08298
111:	28.28439	89.91177	40.46196	52.22254	64.40662
116:	114.96570	93.06992	34.41000	84.12315	76.00535
121:	122.59850	94.00961	76.16579	79.38628	67.82777
126:	44.14775	28.95610	22.63300	8.78925	

Note: The solar constant in *Streamer* calculations that is equal to that calculated for the mean Earth-Sun distance occurs on approximately April 2 and October 4.

The total solar flux of 1354.2 W m^{-2} differs from the typical "solar constant" value of approximately 1370 W m^{-2} (at a mean Earth-Sun distance) because of the difference in the width of the solar spectrum. In *Streamer* the shortwave spectrum covers the wavelengths 0.28 - 4.0 μm. If *Streamer*'s spectrum ranged from 0.2 to 5.0 μm, the total solar flux would be approximately 1367 W m^{-2}.

9 BAND WEIGHTS

Band weights can be used to approximate an instrument's spectral response functions. The structure of the optional file of band weights was described in the *Input* section of the *User's Guide.* Band weights are currently available for the sensors listed in the table below. "KT-19" refers to the Heimann KT19.85 infrared radiometer, which is not a satellite sensor. Other band weights may be available. Check the **bandweights** directory of the program distribution.

Available Sensor Band Weight Files

Platform	Sensor	File
NOAA-12	AVHRR	avhrr-12.wts
NOAA-15	AVHRR	avhrr-15.wts
NOAA-16	AVHRR	avhrr-16.wts
GOES8	imager	goes8_imager.wts
Terra	MODIS	modis.wts
ERS-2	ATSR2	atsr2.wts
MSG	SEVIRI	seviri.wts
---	KT-19	kt19.wts

Figure 20-1 gives an example of the response functions of the AVHRR relative to *Streamer* bands. The table below shows MODIS bandwidths and the corresponding *Streamer* bands. In some cases the channel bandwidth is considerably less than that of the *Streamer* band. In fact, there are cases where more than one channel is contained within the same *Streamer* band (e.g., MODIS bands 17-19 and 20-23). Be extremely careful with these bands, or avoid them altogether! The wider the sensor band, and hence the more *Streamer* bands that it covers, the more accurate is the estimate. Similarly, the differences between modeled AVHRR radiances for the different satellites will probably be within the noise level.

CAUTION

The accuracy of the computed radiances depends upon the width of the sensor channel relative to the width of the *Streamer* bands that cover it. For some sensors more than one channel may fit into a single *Streamer* band. Avoid those cases.

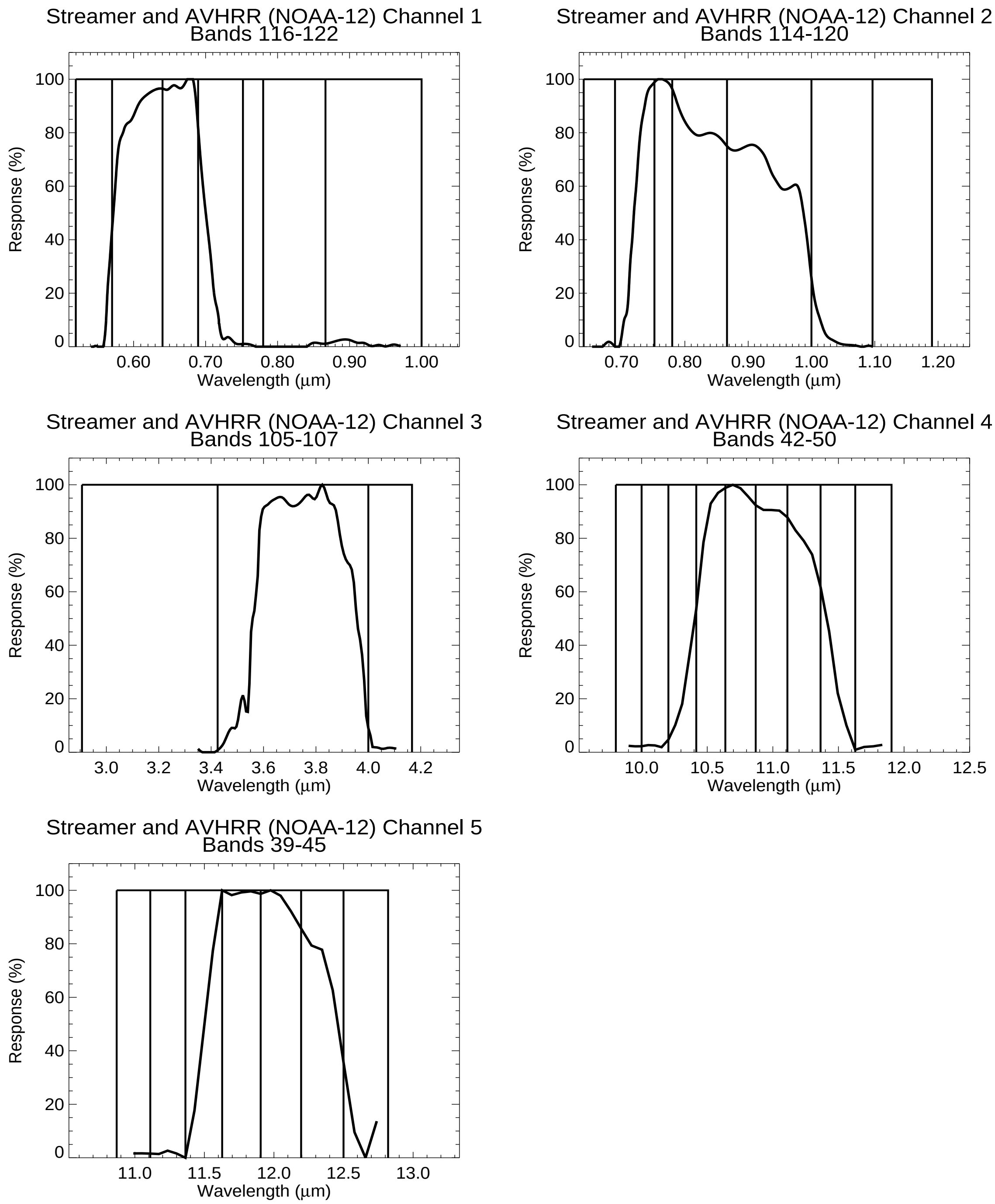

Fig. 9-1. AVHRR (NOAA 7) spectral response functions.

MODIS Bands, at Half-power (50% Response) Bandwidth

Band	Range (µm)	Range (cm-1)	*Streamer* Bands
1	0.62 – 0.67	14925.37 – 16129.03	120 –121
2	0.84 –0.88	11422.04 –11897.68	116 –117
3	0.459 –0.479	20876.83 –21786.49	124
4	0.545 –0.565	17699.12 –18348.62	122
5	1.230 –1.250	8000.00 –8130.08	113
6	1.628 –1.654	6051.44 –6144.39	110 –111
7	2.105 –2.155	4640.37 –4750.59	109 –110
8	0.405 –0.420	23837.90 –24721,88	125
9	0.438 –0.448	22321.43 –22831.05	124
10	0.483 –0.493	20283.98 –20703.93	123
11	0.526 – 0.536	18656.72 – 19011.41	122
12	0.546 – 0.556	17985.61 – 18315.02	122
13	0.662 – 0.672	14880.95 – 15105.74	120
14	0.673 – 0.683	14641.29 – 14858.84	120
15	0.743 – 0.753	13280.21 – 13458.95	118 – 119
16	0.862 – 0.877	11409.01 – 11607.66	116 – 117
17	0.890 – 0.920	10869.56 – 11235.96	116
18	0.931 – 0.941	10626.99 – 10741.14	116
19	0.915 – 0.965	10362.69 – 10928.96	116
20	3.660 – 3.840	2604.17 – 2732.24	106
21	3.930 – 3.989	2507.21 – 2544.85	106
22*	3.930 – 3.989	2507.21 – 2544.85	106
23	4.020 – 4.081	2450.68 – 2487.87	105 - 106
24	4.433 – 4.498	2223.46 – 2256.06	102 – 103
25	4.482 – 4.549	2198.53 – 2231.40	102
26	1.360 – 1.390	7194.24 – 7342.94	112
27	6.535 – 6.895	1450.33 – 1530.22	72 –76
28	7.175 – 7.475	1337.79 – 1393.73	66 – 69
29	8.400 – 8.700	1149.43 – 1190.48	57 – 59
30	9.480 – 9.980	1002.00 – 1054.85	50 – 52
31	10.78 – 11.28	886.52 – 927.64	44 – 46
32	11.77 – 12.27	815.00 – 849.62	40 – 42
33	13.19 – 13.49	741.56 – 758.44	37
34	13.49 – 13.79	725.43 – 741.56	36 – 37
35	13.79 – 14.09	709.98 – 725.43	35 – 36
36	14.09 – 14.39	695.17 – 709.98	34 – 35

* The design of channels 21 and 22 is such that they have different saturation levels (no difference here).

10 REFERENCES

Blanchet, J-P and R. List, 1983, Estimation of optical properties of Arctic haze using a numerical model, *Atmosphere-Ocean*, 21(4), 444-465.

Brieglieb, B.P., P. Minnis, V. Ramanathan, and E. Harrison, 1986, Comparison of regional clear-sky albedos inferred from satellite observations and model computations, *J. Clim. Appl. Meteorol.*, 25, 214-226.

Cess, R.D., 1985, Nuclear war: Illustrative effects of atmospheric smoke and dust upon solar radiation, *Clim. Change*, 7, 237-251.

Domingue, D., B. Hartman, and A. Verbiscer, 1997, The scattering properties of natural terrestrial snows versus icy satellite surfaces, *Icarus*, 128, 28-48.

Ebert, E.E. and J.A. Curry, 1992, A parameterization of ice cloud optical properties for climate models, *J. Geophs. Res*., 97(D4), 3831-3836.

Ellingson, R.G., J. Ellis, and S. Fels, 1991, The intercomparison of radiation codes used in climate models: long wave results, *J. Geophys. Res*., 96(D5), 8929-8953.

Fu, Q. and K.N. Liou, 1993, Parameterization of the radiative properties of cirrus clouds, *J. Atmos.Sci.*, 50(13), 2008-2025.

Fu, Q. and K.N. Liou, 1992, On the correlated k-distribution method for radiative transfer in non-homogeneous atmospheres, *J. Atmos. Sci*., 49, 2139-2156.

Grenfell, T.C. and G.A. Maykut, 1977, The optical properties of ice and snow in the arctic basin, *J. Glaciol.*, 18(80), 445-463.

Hapke, B.W., 1981, Bidirectional reflectance spectroscopy, 1: Theory, *J. Geophys. Res.*, 86, 3039-3054.

Hu, Y.-X., B. Weilicki, Lin, G. Gibson, S.-C. Tsay, K. Stamnes, and T. Wong, 2000, Delta-Fit: A fast and accurate treatment of particle scattering phase functions with weighted singular-value decomposition least-squares fitting, *J. Quant. Spect. & Rad. Trans*., 65, 681-690.

Hu, Y.X. and K. Stamnes, 1993, An accurate parameterization of the radiative properties of water clouds suitable for use in climate models, *J. Climate*, 6(4), 728-742.

Key, J., P. Yang, B. Baum, S. Nasiri, 2001, A parameterization of ice cloud optical properties for various particle habits, J. Geophysical Research, in preparation.

Kidwell, K.B. (ed.), 1991, NOAA polar orbiter data user’s guide, NOAA/NESDIS.

Kylling, A., K. Stamnes, and S.-C. Tsay, 1995, A reliable and efficient two-stream algorithm for spherical radiative transfer: documentation of accuracy in realistic layered media, *J. Atmos. Chem.*, 21, 115-150.

Kneizys, F.X., Shettle, E.P., Abreu, L.W., Chetwynd, J.H, Anderson, G.P., Gallery, W.O., Selby, J.E.A., Clough, S.A., 1988, Users Guide to LOWTRAN7. Environmental Research Papers, No. 1010, AFGL-TR-88-0177, Air Force Geophysics Laboratory, Hanscom AFB, Massachusetts, 137 pp.

Minnaert, M., 1941, The reciprocity principle in lunar photometry, *Astrophys. J*., 93, 403-410.

Nakajima, T. and M. Tanaka, 1988, Algorithms for radiative intensity calculations in moderately thick atmospheres using a truncation approximation, *J. Quant. Spectrosc. Radiat. Transfer,* 40, 51-69.

Rahman, H., B. Pinty, and M.M. Verstraete, 1993, Coupled surface-atmosphere reflectance (CSAR) model 2. Semiempirical surface model usable withNOAA advanced very high resolution radiometer data, *J. Geophys. Res.*, 98(D11), 20791-20801.

Roujean, J-L., M. Leroy, and P-Y. Deshamps, 1992, A bidirectional reflectance model of the earth's surface for the correction of remote sensing data, *J. Geophys. Res.*, 97(D18), 20455-20468.

Pinty, B. and M.M. Verstraete, 1991, Extracting information on surface properties from bidirectional reflectance measurements, *J. Geophys. Res.*, 96(D2), 2865-2874.

Schmidt, E.O., R.F. Arduini, B.A. Wielicki, R.S. Stone, and S.-C. Tsay, 1995, Considerations for modeling thin cirrus effects via brightness temperature differences, *J. Appl. Meteorol.*, 34(2), 447-459.

Slingo, A. and H.M. Schrecker, 1982, On the shortwave radiative properties of stratiform water clouds, *Quart. J. Roy. Meteor. Soc.*, 108, 407-426.

Shettle, E.P. and R.W. Fenn, 1979, Models for the aerosols fo the lower atmosphere and the effects of humidity variations on their optical properties, Environmental Research Papers, No. 676, AFGL-TR-79-0214, USAF, 94 pp.

Snell, H.E., Anderson, G.P., Wang, J., Moncet, J.-L., Chetwynd, J.H., and English, S.J., 1995, Validation of FASE (FASCODE for the environment) and MODTRAN3: Updates and comparisons with clear-sky measurements. *SPIE Conference 2578 Proceedings*, Paris, 194-204.

Stamnes, K., S.C. Tsay, W. Wiscombe and K. Jayaweera, 1988, Numerically stable algorithm for discrete-ordinate-method radiative transfer in multiple scattering and emitting layered media, *Appl. Opt.*, 27, 2502-2509.

Stamnes, K., S-C. Tsay, and W. Wiscombe, 1994, A general-purpose, numerically stable computer code for discrete-ordinate-method radiative transfer in scattering and emitting layered media, Part I: documentatin of methodology, 62 pp.

Stamnes, K., S.C. Tsay, W. Wiscombe and I. Laszlo, 2000, A General-Purpose Numerically Stable Computer Code for Discrete-Ordinate-Method Radiative Transfer in Scattering and Emitting Layered Media, DISORT Report v1.1.

Stephens, G.L., 1979, Optical properties of eight water cloud types, CSIRO Aust. Div. Atmos. Phys. Tech. Pap. No. 36, 35 pp.

Takano, Y. and K.-N. Liou, 1989, Solar radiative transfer in cirrus clouds. Part I: Single-scattering and optical properties of hexagonal ice crystals, *J. Atmos. Sci.*, 46(1), 3-19.

Tanre, D. et al., 1986, Simulation of the satellite signal in the solar spectrum (5S), Laboratoire d'Optique Atmospherique, 262 pp.

Toon, O.B. C.P. McKay, and T.P. Ackerman, 1989, Rapid calculation of radiative heating rates and photodissociation rates in inhomogeneous multiple scattering atmospheres. *J. Geophys. Res.*, 94(D13), 16287-16301.

Tsay, S.-C., K. Stamnes and K. Jayaweera, 1989: Radiative energy budget in the cloudy and hazy Arctic. *J. Atmos. Sci.*, 46,1002-1018.

Tsay, S.-C., K. Stamnes, and K. Jayaweera, 1990, Radiative transfer in stratified atmospheres: development and verification of a unified model, *J. Quant. Spectrosc. Radiat. Transfer*, 43, 133-148.

Tsay, S-C. and G. L. Stephens, 1990, A physical/optical model for atmospheric aerosols with application to visibility problems, Department of Atmospheric Sciences, Colorado State University, Fort Collins, Colorado,65 pp., ISSN 0737-5352-16.

Verbiscer, A.J. and J. Veverka, 1990, Scattering properties of natural snow and frost: Comparison with icy satellite photometry, *Icarus*, 88, 418-428.

Vermote, E., Tanre, D., Deuze, J.L., Herman, M., and Morcrette, J.J., 1994, Second Simulation of the Satellite Signal in the Solar Spectrum (6S): User Guide.Laboratoire d'Optique Atmospherique, Universite des Sciences et Technologies de Lille, France, 216 pp.

Warren, S.G. and W.J. Wiscombe, 1980: A model for the spectral alpedo of snow II. Snow containing atmospheric aerosols. *J. Atmos.Sci.*, 37, 2734-2745.

Wiscombe, W.J., and J.W. Evans, 1977, Exponential-sum fitting of radiative transmission functions, *J. Computational Physics*, 24, 416-444.

11 REVISION HISTORY

This table shows major and secondary revisions. Minor revisions are not listed. "B" is beta test; “p” means preliminary.

Version	Date	Changes
3.0b	1 March 2001	Incorporated new version of DISORT (v2.0); added eight ice particle habit optical property models; added capability to input surface bidirectional reflectance and added BRDF models; added capability to input cloud optical properties, including a phase function; added one snow surface type; added the option of specifying spectral range with wavelengths, wavenumbers, or band numbers; added defaults file alternative to editing **defaults.f** and recompiling; changed cloud input format to allow for the calculation of water content based on optical and geometrical thickness; switched to the double Henyey-Greenstein function for ice clouds in the shortwave with more than two streams; added an interactive mode of operation and the commands $ASSIGN, $LOAD, $RUN, and $EXIT; input unit variables are now replaceable; eliminated backspacing with $replace; changed the structure of the default input file and added a command line option to specify a defaults file; added band weights for more sensors. Input format and features are different; see the file **input_2vs3.txt** for details.
2.6	26 October 1999	Replaced IDL GUI with an HTML interface; added an HTML version of the manuals; added grass, dry grass, deciduous, and coniferous vegetation albedo types and replaced the generic vegetation type with the average of these; redid the longwave ice cloud parameterization down to 5 micron Re; added KT19 band weights.
2.5	9 March 1999	Adjusted CO_2 amount to approx. 355 ppm; added parallel loop structure in $REPLACE; added automatic conversion of satellite scan angles.
2.4p	8 September 1998	Added mixed-phase cloud optical property parameterization.
2.3p	15 July 1998	Replaced Ebert and Curry shortwave ice cloud parameterization with Fu and Liou.
2.2p	15 April 1998	Further improved the IDL GUI; replaced the solar flux data; added a solar flux adjustment for Earth-Sun distance.
2.1p	28 August 1996	Completed Beta testing of cloud overlap.

2.1pB	10 June 1996	Added output for total shortwave and net fluxes; added heating/cooling rate, increased max line length for $REPLACE; removed IDL interface (at least temporarily); modified cloud overlap to allow for 10 overlap sets and 10 overlapping clouds; developed a **streamer** subroutine; corrected bug in open water albedo routine; removed command line options capability, removed cloud model definition from options and added it to the input data; increased the maximum number of polar and azimuthal angles. The input file is not backward compatible.
2.00p	15 Apr 1994	Changed interface (added $EXCHANGE, $OPTIONS, $PRINT, $COMMENT), added other aerosol models, broadband albedo input, “missing” cloud top temperatures, cloud bottom option, added heating rates to flux output, added IDL interface, added DISORT version 2 (preliminary, not complete), replaced water cloud parameterization.
1.22	13 Dec 1993	Changed the computation and output of satalb & sattb; created the READRAW utility.
1.2	6 Dec 1993	Added: user output option, standard profiles, “$replace” input option; MODIS & HIRS weights.
1.1	18 Oct 1993	Changed method of specifying standard profiles and surface fractions; modified the way band 106 is treated (radiances)
1.0	16 Sep 1993	Added the weighting function option
1.0B	1 Jul 1993	First public Beta test version
0.0	1992	Development of *Streamer* begun with a version of Si-Chee Tsay’s *strats* program that had been modified by A. Schweiger and J. Key (modified for A. Schweiger’s dissertation research).